Ab initio Calculation of the Electronic Structure of the Strontium Hydride Ion (SrH+)

ARTICLE *in* INTERNATIONAL JOURNAL OF QUANTUM CHEMISTRY · FEBRUARY 2015

Impact Factor: 1.43 · DOI: 10.1002/qua.24813

6 AUTHORS, INCLUDING:

Héla Habli

University of Monastir

9 PUBLICATIONS **31** CITATIONS

SEE PROFILE

Noureddine Issaoui

University of Monastir

26 PUBLICATIONS **66** CITATIONS

SEE PROFILE

Brahim Oujia

University of Monastir

61 PUBLICATIONS **297** CITATIONS

SEE PROFILE

Florent Xavier Gadéa

Paul Sabatier University - Toulouse III

153 PUBLICATIONS **2,824** CITATIONS

SEE PROFILE

Ab initio Calculation of the Electronic Structure of the Strontium Hydride Ion (SrH^+)

Héla Habli,*[a] Leila Mejrissi,[a] Noureddine Issaoui,[a] Saud Jamil Yaghmour,[b] Brahim Oujia,[a,b] and Florent Xavier Gadéa[c]

The potentials, spectroscopic properties and electric dipole moments of SrH^+ are computed for 63 molecular states dissociating up to $Sr^{2+} + H^-$ using an *ab initio* approach. The *ab initio* formalism is based on large basis sets, nonempirical atomic pseudopotential for strontium core, correlation treatment for core valence through the effective core polarization potentials and for valence through full valence configuration interaction. Our theoretical molecular constants match published values very well and a large amount of new results is produced. Unusual potential shapes are found in $^1\Sigma^+$ states often caused by avoided crossing series between them and imprinted by the ionic state $Sr^{2+}H^-$. The high potential energy curves suggest, it is possible to form H^- or at least to neutralize H^+ in collisions with strontium. © 2014 Wiley Periodicals, Inc.

DOI: 10.1002/qua.24813

Introduction

There is a considerable interest in studies on alkaline earth hydrides (YH)[1–8] and their corresponding cations (YH^+),[9–27] where Y = Ba, Sr, Ca, Mg, and Be. They are important systems in astrophysics and spectroscopy due to their visible bands which emerge in the absorption spectrum of several stars and of the Sun.[28–33] For instance, the magnesium isotope abundances in various astronomical elements are estimated regularly by the use of the green bands of magnesium hydride molecule.[34] Furthermore, Johnson and Sauval[35] noticed the YH^+ ionic system existing in the red-giant stars. The knowledge of their molecular constant usually helps to design circum-stellar media models around cool stars.[36–40] In addition, the solar abundance of Y (Y = Ba, Mg,. . .) atoms was measured through the broadening study of Y^+ lines by collisions with hydrogen.[41,42] In this framework, numerous calculations of the solar abundance of strontium have mentioned that Sr atom emerges mainly in the first ionization state.[42] In these broadening studies, the higher states of the YH system are of paramount importance. Experimentally, Mølhave and Drewsen[43] proved that the creation of alkaline earth monohydrides ion is possible in a linear Paul trap with laser-cooled atomic cations. The cooling laser excites the atomic cations that easily react with the gas molecules purposely put in the background.[44] Using laser-cooled atomic ions Kosloff and coworkers[45,46] investigated the photodissociation of magnesium hydride cation embedded in Coulomb crystals.

Motivated by the numerous experimental works on alkaline earth hydrides cation, numerous theoretical investigations have been performed for YH^+ systems.[9–27] Both adiabatic potential energy and dipole moments of these diatomic hydride cations have been investigated by various numerical methods. The assignments of the low-lying higher states have been confirmed experimentally. Among the various *ab initio* calculation for the first state $X^1\Sigma^+$ of these ionic systems, the spectroscopic constants of BaH^+ calculated by Mejrissi et al.[14] meet the best agreement with experimental data.

Several electronic structure investigations have been theoretically performed for SrH^+.[22–26] However, most of them have studied only the ground electronic state $X^1\Sigma^+$. The first work was done by Fuentealba and Schilling in 1987. They have computed the molecular spectroscopic constants for $X^1\Sigma^+$. Then, Abe et al.[24] have computed the properties of $X^1\Sigma^+$ of several alkaline earth hydride cations by MOLCAS software (version 7.2) with a high-quality basis set. To evaluate Stark shifts linked, the dipole moment properties of the $X^1\Sigma^+$ state have been determined for these cations. Only recently, Aymar and Dulieu,[22] have investigated the first fourth excited states for CaH^+, BaH^+, MgH^+, and SrH^+ using a full valence configuration interaction (FCI) method. Experimentally, the properties for SrH^+ have been rarely investigated except for $X^1\Sigma^+$ dissociation energy[23] evaluated in collisional process.

In this study, we perform a wide adiabatic investigation of SrH^+ system and calculate almost all potential energy curves (PECs) dissociating below the $Sr^{2+} + H^-$ limit. The 34 $^{1,3}\Sigma^+$, 20 $^{1,3}\Pi$, and 9 $^{1,3}\Delta$ states are treated following a Born Oppenheimer approach. In addition, we analyze for the first time both the transition (TDM) and permanent (PDM) dipole

[a] *Héla Habli, L. Mejrissi, N. Issaoui and B. Oujia*
Laboratoire de Physique Quantique, Faculté des Sciences de Monastir, Université de Monastir, Avenue de l'Environnement 5019, Monastir, Tunisie
E-mail: hablihela@gmail.com
[b] *S. J. Yaghmour and B. Oujia*
King Abdulaziz University, Faculty of Science, Department of Physics, Jeddah, Kingdom of Saudi Arabia
[c] *F. X. Gadéa*
Laboratoire de Chimie et Physique Quantique, UMR5626 du CNRS, Université de Toulouse, UPS, 118 route de Narbonne, 31062, Toulouse Cedex 4, France

moments. The spacing of vibrational levels is also presented for nearly all these electronic states. This latter determination gives very useful information to discuss the anomalous behavior for the higher excited states. For $X^1\Sigma^+$, several theoretical and experimental investigations[22–27] for the electronic and electric properties have been undertaken in the past. Our results are compared to the available works for the lower states. The higher excited states are investigated here for the first time.

Theory and Computational Details

Computational procedure

In this section, we recall the most important lines of the methods used here for the structure calculation of the SrH^+ molecular ion. This system, composed of 38 electrons, is considered as a two effective electron system taking benefit of the shape consistent relativistic pseudopotential technique developed by Durand and Barthelat[47,48] and used in several studies.[14–16,49] In this study, the electronic energy was determined first at the self-consistent field including the core valence electron correlation with with effective core potential (ECP), core polarization potentials (CPP) methods and FCI calculations using the package codes of Toulouse.[9,14–16,18,19,47–59] In this study, we report new results which characterize highly electronic states below the $(Sr^{2+} + H^-)$ limit extending the work of Aymar and Dulieu[22] focusing on (X-E) states.

To supply the fixed core approximation inherent to the pseudopotential approach, core valence correlation has been estimated according to the Muller formalism[60] with the CPP operator:

$$V_{\text{cpp}} = -\frac{1}{2}\sum_c \alpha_c \vec{f}_c . \vec{f}_c \tag{1}$$

In this expression, α_c presents dipole polarizability of the core c. The strontium core polarizability used here is $\alpha_{Sr} = 5.67a_0^3$[61] similarly to Aymar and Dulieu[22] $\vec{f}_c$ represents the electrostatic field, which can be created by all other center cores and the valence electrons at center c. It is expressed as follows:

$$\vec{f}_c = \sum_i \frac{\vec{R}_{ci}}{R_{ci}^3} F(R_{ci}, \rho_c) - \sum_{c' \neq c} z_c \frac{\vec{R}_{c'c}}{R_{c'c}^3} \tag{2}$$

The $\vec{R}_{ci}$ and $\vec{R}_{c'c}$vectors are, respectively, the core–electron and core–core vectors. Using the l-dependent cutoff functions,[62] the cutoff operator $F_l(R_{ci}, \rho_c)$ is given with a step function:

$$F_l(R_{ci}, \rho_c) = \begin{cases} 1 \text{ if } R_{ci} > \rho_c \\ 0 \text{ if } R_{ci} < \rho_c \end{cases} \tag{3}$$

The ρ_c parameter is defined by the following function:

$$F(R_{ci}, \rho_c) = \sum_{l=0}^{\infty} \sum_{m=-l}^{+l} F_l(R_{ci}, \rho_c) |lmc\rangle\langle lmc| \tag{4}$$

The operator $(|lmc\rangle\langle lmc|)$ describes the spherical harmonics centered at the c core.

As pointed out in the work of Habli et al.,[15] the l-dependent CPP approach with several cutoff radii leads to an incorrect asymptotic behavior possibly caused by an underestimation of nuclear and electronic fields associated to the truncation in the l-expansion. We, therefore, used here the CPP l-independent form and a single cutoff radius (ρ_{Sr}) in the spherical function $F(R)$[52,60,63]:

$$F = \left[1 - \exp\left(-\frac{R_{ci}^2}{\rho_c^2}\right)\right] \tag{5}$$

This ρ_{Sr} parameter varies considerably with the basis functions. The ρ_{Sr} parameter is adjusted to reproduce the binding energies for the first atomic levels of Sr^+ (5s) (second ionization potential) and we get the $\rho_{Sr} = 2.3995$ a.u. value.

Basis sets optimization

The exploration of the highly excited molecular states requires large Gaussian-type orbitals (GTO) basis sets both for the strontium and for the hydrogen atoms since many configurations are investigated.

For the strontium ion, we optimized an extended uncontracted basis set (8s6p6d) composed of 56 functions with the diffuse orbital exponents tuned to reproduce the involved atomic levels of Sr^+ (5s, 6s, 7s, 8s, 9s, 5p, 6p, 7p, 8p, 4d, 5d, 6d, and 7d) and of Sr ($5s^2$, 5s5p and 5s4d). It matches around 20 atomic levels of the Sr and Sr^+ with good accuracy and is flexible enough to treat molecular effects.

For the H atom, we use the (8s5p3d/5s2p2d) basis set optimized in our previous works.[14] The number of GTO functions is reduced to only 21. It matches the various energies of H (1s, 2s, and 2p) and H^-.

The computed level energies as well the experimental data[64] are displayed in Table 1, for Sr^+, Sr, and H. To compare with the experimental data, the dissociating limit energy of $(Sr^{2+} + H^-)$ is defined as $(PI_{SrI} + PI_{SrII} + E_H - EA_H)$, where PI_{SrI}(=545932.20 cm^{-1})[64] and PI_{SrII}(= 88965.18 cm^{-1})[64] are, respectively, the ionization potentials SrI and SrII. E_{H+} is the ionization energy of Hydrogen (109733.92 cm^{-1})[64], and EA_H(=6083 cm^{-1})[65] is the electron affinity of hydrogen. Table 1 shows that for both Sr^+ and H, the discrepancy between the experimental energies and ours does not exceed 50 cm^{-1} except for the Sr^+(9s), Sr^+(6d), and Sr^+(7d) states. For the strontium atom, the maximum error is around 600 cm^{-1}. For the strontium hydride ion, all molecular energies levels below $(Sr^{2+}\ H^-)$ limit are, thus, reproduced rather accurately. From Table 1, it can be checked that the relative error between our results and the experiments are far below 0.5% and thus acceptably small. For the 11 lowest asymptotic limits, there is a very good agreement. The largest difference is about of few tens of wave numbers for (Sr^+ (7d) + H(1s)), (Sr (5s5p) + H^+), and (Sr (5s4d) + H^+) limits. This good agreement with the experimental data gives reliability to our calculation method and validates the basis set optimization.

Table 1. Theoretical and experimental energies level spectrum for $Sr^+(E^+_{Sr}-E^{2+}_{Sr})$, $Sr(E_{Sr}-E^+_{Sr}-E^{2+}_{Sr})$, and $H(E_H-E^+_H)$ and the error (ΔE_1) in cm^{-1}.

Strontium ion				Strontium			
Atomic levels	Exp[64]	This work	ΔE_1	Atomic levels	Exp[64]	This work	ΔE_1
5s	−88964.88	−88964.88	0.00	$5s^2$	−134896.84	−135191.81	294.97
6s	−41228.41	−41226.65	1.76	5s5p	−120194.27	−120740.11	545.84
7s	−23999.92	−24000.35	0.46	5s4d	−116643.19	−116026.91	616.28
8s	−15726.84	−15726.62	0.22				
9s	−11107.53	−10944.73	162.80				
5p	−64715.42	−64716.42	1.00				
6p	−33002.30	−33005.80	3.50	Hydrogen			
7p	−20192.92	−20194.42	1.50	1s	−109733.92	−109726.12	7.8
8p	−13652.33	−13475.33	177	2s	−27474.98	−27430.37	44.6
4d	−74239.71	−74260.71	21.00	2p	−27241.71	−27427.08	47.69
5d	−35626.55	−35634.25	7.70	H^+	−115816.86	−115416.32	400.54
6d	−21148.07	−21413.07	265.00				
7d	−14330.55	−13786.55	544.00				

Molecular limits

Asymptotes	Exp[64] (cm^{-1})	This work (cm^{-1})	ΔE/E	Molecular states
Sr^+ (5s)+H (1s)	−198698.80	−198691.00	0.392	$^{1,3}\Sigma^+$
Sr^+ (4d)+H (1s)	−183973.63	−183986.83	−0.717	$^{1,3}\Sigma^+$, $^{1,3}\Pi$, $^{1,3}\Delta$
Sr^+ (5p)+H (1s)	−174449.34	−174442.54	0.389	$^{1,3}\Sigma^+$, $^{1,3}\Pi$
Sr^+ (6s)+H (1s)	−150962.33	−150952.77	0.634	$^{1,3}\Sigma^+$
Sr^+ (5d)+H (1s)	−145360.47	−145360.37	0.007	$^{1,3}\Sigma^+$, $^{1,3}\Pi$, $^{1,3}\Delta$
Sr^+ (6p)+ H (1s)	−142736.22	−142731.92	0.301	$^{1,3}\Sigma^+$, $^{1,3}\Pi$
Sr ($5s^2$)+H^+	−134896.84	−135191.81	−21.866	$^1\Sigma^+$
Sr^+ (7s)+H (1s)	−133733.84	−133726.47	0.551	$^{1,3}\Sigma^+$
Sr^+ (6d)+ H (1s)	−130881.99	−131139.19	−19.651	$^{1,3}\Sigma^+$, $^{1,3}\Pi$, $^{1,3}\Delta$
Sr^+ (7p)+H (1s)	−129926.84	−129920.54	0.485	$^{1,3}\Sigma^+$, $^{1,3}\Pi$
Sr^+ (8s)+H (1s)	−125460.76	−125452.74	0.639	$^{1,3}\Sigma^+$
Sr^+ (7d)+H (1s)	−124064.47	−123512.67	44.475	$^{1,3}\Sigma^+$, $^{1,3}\Pi$, $^{1,3}\Delta$
Sr^+ (8p)+H (1s)	−123386.25	−123201.45	14.977	$^{1,3}\Sigma^+$, $^{1,3}\Pi$
Sr^+ (9s)+H (1s)	−120841.45	−120670.85	14.117	$^{1,3}\Sigma^+$
Sr (5s5p)+H^+	−120194.27	−120740.11	−45.413	$^3\Sigma^+$, $^3\Pi$
Sr (5s4d)+H^+	−116643.19	−116026.91	52.834	$^3\Sigma^+$, $^3\Pi$, $^3\Delta$
Sr^+ (5s)+H (2s)	−116439.86	−116395.25	3.831	$^{1,3}\Sigma^+$
Sr^+ (5s)+H (2p)	−116206.59	−116391.96	−15.951	$^{1,3}\Sigma^+$, $^{1,3}\Pi$
Sr^{2+} +H^-	−115816.92	−115416.32	34.580	

Molecular limits of the ion SrH^+ and relative error ($\times 10^2$) (ΔE/E)

Results and Discussions

Electronic energy curves

Using this quantum chemistry approach based on pseudo potentials for the strontium core complemented by CPP and FCI, we have computed the adiabatic PECs for the $^{1,3}\Sigma^+$, $^{1,3}\Pi$, and $^{1,3}\Delta$ states up to the $Sr^{2+}+H^-$ limit. These curves are shown in Figures 1–4. They have been computed for interatomic distances ranging from 2.5 up to 200 a.u.

In Figures 1a and 1b, we noted interesting behaviors for the excited states of $^1\Sigma^+$ symmetry. The first states present a rather simple shape, for example, the $X^1\Sigma^+$, $A^1\Sigma^+$ and $C^1\Sigma^+$ states are found with a single minimum at 3.72, 4.64 and 5.77 a.u., respectively. While, the behavior of the higher molecular states is more complex: series of undulations can be seen in this figure. These undulations lead to potentials with multiple wells (double, triple,...) and interesting spectroscopic signatures can be expected. For example, the $F^1\Sigma^+$ and $G^1\Sigma^+$ states have a double minimum at wide distances (13.62 and 15.51 a.u., respectively) and another at short distances (4.64 and 5.46 a.u., respectively) and their shape results from involved couplings around the avoided crossing. Interestingly, the singlet states of symmetry Σ^+ are all attractive as they have at least one potential well. Moreover, the very attractive curve can be explained through the presence of several avoided crossing originating from the shape of the ionic charge transfer state (Sr^{2+} H^-) which behaves as (−2/R). Thus, we can understand the formation of potentials with multiple wells.

In Supporting Information, Table S1, we listed the positions of such avoided crossing with their corresponding energy difference. Interestingly, important consequences can be deduced from these crossing associated to the excitation or charge transfer efficiency. For instance, we can mention the neutralization cross-sections, which depend critically of the positions of the avoided crossing series and their great importance for charge transfers in diverse astrophysical environments.[66–69] From

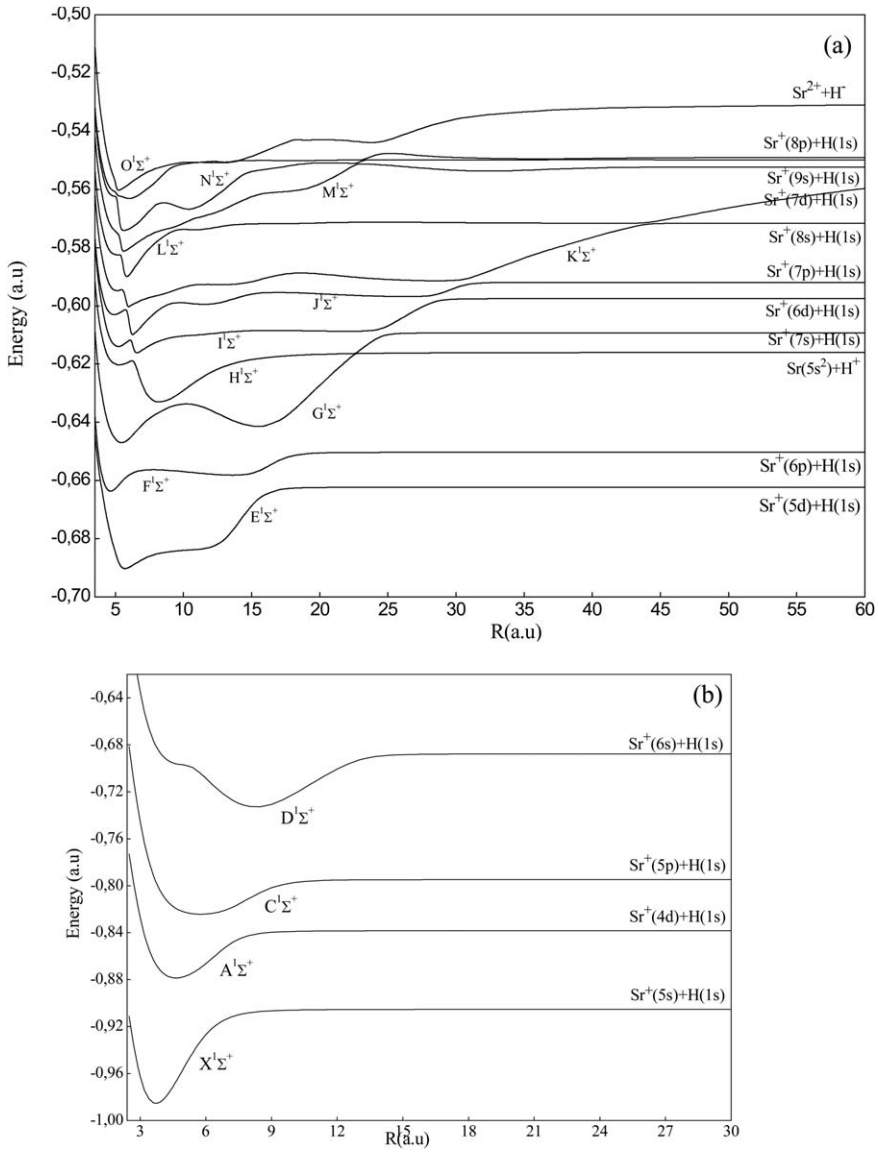

Figure 1. Adiabatic $^1\Sigma^+$ potential energy curves: (a) for $X^1\Sigma^+$, $A^1\Sigma^+$, $C^1\Sigma^+$, and $D^1\Sigma^+$ states and (b) for higher excited states of $^1\Sigma^+$ dissociating below the ionic limit Sr^{2+} H^-.

Figures 1a and 1b, we can deduce various possible processes during collisions between H^+ and strontium by inspecting the higher PECs. For example, a diabatic passage could be carried at the vicinity of the avoided crossing G–H, due to the very weakly coupling, however, at short distances larger couplings are experimented and charge transfer to Sr*H may be anticipated. Furthermore, on the way out, the stronger couplings can be found between the Sr*H states and the $Sr^{2+}H^-$ ionic state. Therefore, neutralization or even H^- formation seems possible from a single collision of H^+ with the strontium atom.

In the high energy part, at short distances, there is also another series of avoided crossing with now a very repulsive underlying state. This state could be related to Sr $(5s^2) + H^+$ since all the other states in this energy range dissociate to $Sr^{*+} + H$ and are not expected to be extremely repulsive.

In Figures 2a and 2b, we display the shape of the PECs for the $^3\Sigma^+$ symmetry. The three lowest states have shallow wells at unusually large distances, while the higher ones have a similar behavior to the singlet states, with a deep well at short distance and often another one at large internuclear distances. For instance, three avoided crossing between (k and l) $^3\Sigma^+$ states are observed leading to anomalous behavior in their PECs. We note the existence of two series of avoided crossing with underlying states which behave like ionic ones. Hylleraas[70] also found the existence of excited triplet states of H^-. H^- is the simplest two electron system and the normalized ground state electron affinity of the H atom is a fundamental measure of electron correlations.

The PDM will help in the analysis. There is also at short distances an avoided crossing series caused by an underlying repulsive state. Again, this state, more repulsive than the others, could be the one dissociating to H^+, here Sr^+ (5s4d) + H^+. Rich and interesting spectroscopy as well as excitation and charge transfers in collisions are thus expected here also.

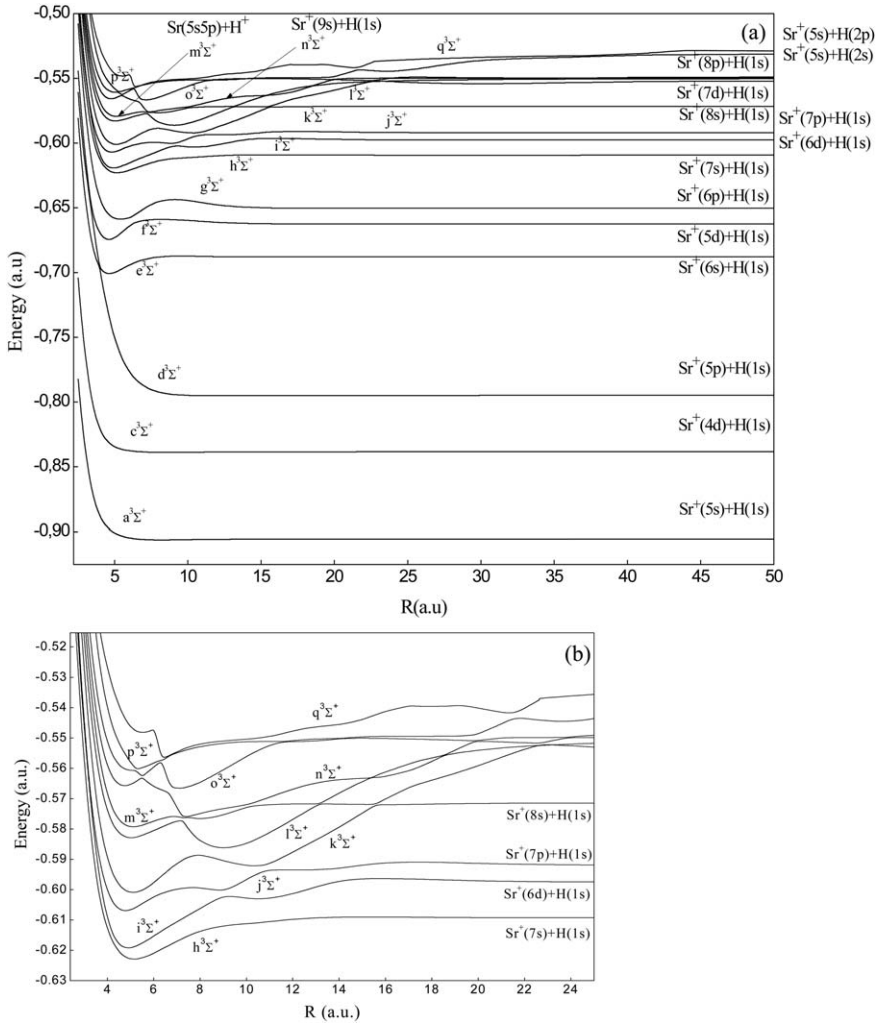

Figure 2. (a) Adiabatic potential energy curves for all excited states of $^3\Sigma^+$ dissociating below the ionic limit Sr^{2+} H^- and (b) Zoom for the higher excited $^3\Sigma^+$ states.

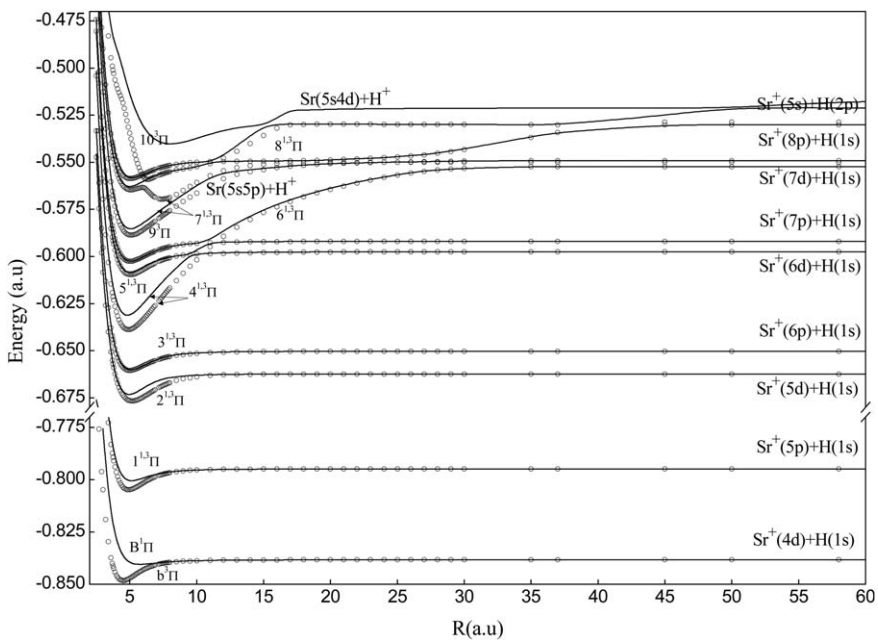

Figure 3. $^1\Pi$ (Solid lines) and $^3\Pi$ (circle lines) adiabatic potential energy curves.

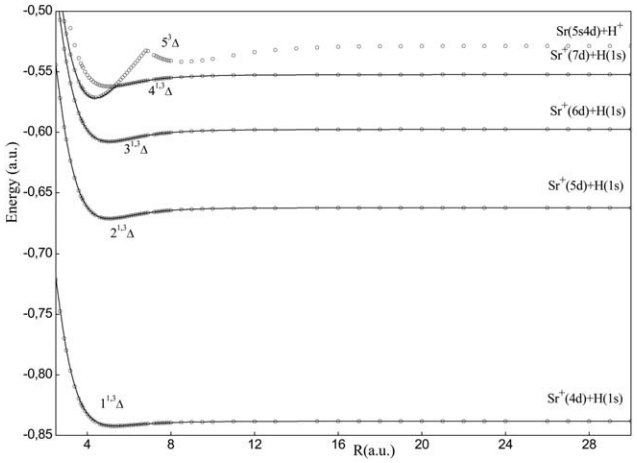

Figure 4. $^1\Delta$ (solid lines) and $^3\Delta$ (circle lines) adiabatic potential energy curves.

For the symmetry $^{1,3}\Pi$, the PECs for 20 states are drawn from 2.5 to 60 a.u. in Figure 3. Several potentials exhibit an attractive character where the singlet states are slightly less deep than the triplet states, like in atoms. Series of avoided crossing similar to that seen for the $^{1,3}\Sigma^+$ states can be seen for the higher excited states of symmetry $^{1,3}\Pi$, suggesting again surprisingly ionic states with H^- in unexpected symmetry $^{1,3}\Pi$.

Comparing Figures 2a and 2b, and 3 it is worth to notice that the lower $^3\Sigma^+$ sates are flat or repulsive while $^1\Pi$, and moreover, $^3\Pi$ ones present deep wells. Similar behavior was observed for the alkali hydride series also a two electron system and was interpreted using the Fermi model as resulting from two effects acting in opposite directions. This system can be considered as an ionic core, here $Sr^{2+}+H$, and a Rydberg electron. The interaction between the H atom and the Rydberg electron is repulsive and more repulsive for Singlet states than for Triplet states, while the ionic core leads to an underlying attractive potential. For the lower $^3\Sigma^+$ states, there is a strong overlap between the H atom and the Rydberg functions oriented along the molecular axis and the two effects compensate, while for the Π states, Rydberg functions perpendicular to the molecular axis are involved and the repulsive interaction with H is lowered, particularly for the triplet states. These arguments also explain why $a^3\Sigma^+$, $c^3\Sigma^+$, and $d^3\Sigma^+$ states are less attractive than the ones higher in energy, they present stronger repulsive interaction with H due to higher density in the corresponding Rydberg functions.

Figure 4 illustrates the PECs for the (1–9) Δ states for interatomic distances R between 2.5 and 30 a.u. These electronic states rather rapidly reach their dissociation limit (typically at distance about 16 a.u.) and the $^{1,3}\Delta$ curves with the same dissociation limit are almost degenerate. Again, in the high energy part some avoided crossing can be seen.

Globally, for all symmetries, the few lowest states ($5^{1,3}\Sigma^+$, $3^{1,3}\Pi$, and $2^{1,3}\Delta$) have the same shape than those determined in Ref. [22] while the higher states are investigated here only. In short, many avoided crossing related to underlying charge transfer states can be clearly observed for all states of symmetry Σ^+ and also Π. They lead to undulating behaviors for the highly excited states at large and intermediate internuclear coordinates and could generate large nonadiabatic couplings. A similar behavior was observed for the CaH^+,[15] BaH^+,[14] and MgH^+[59] and trough rather simple considerations, the apparently strange behavior of the adiabatic states can be analyzed.

Spectroscopic constants

For almost all adiabatic states, the vibrational levels have been investigated with standard methods for solving the 1D Schrödinger equations. To derive the usual molecular spectroscopic constants, we have fitted by least squares method the vibrational level progression using least squares process.

The vibrational level progression is written as follows:

$$E_v = \omega_e - 2\omega_e\chi_e\left(v+\frac{1}{2}\right)+3\omega_e y_e\left(v+\frac{1}{2}\right)^2 \quad (6)$$

These molecular parameters are listed together with the available experimental and theoretical works[22–26] in Table 2 (a–d). The molecular constants are the equilibrium distance (R_e), the potential well depth (D_e), the vertical transition energy (T_e), the equilibrium vibrational pulsation (ω_e), the anharmonic constant ($\omega_e\chi_e$), and the rotational constant (B_e).

For the ground state, there is only one experimental study.[23] As can be seen in Table 2 (a), our well depth is in excellent agreement with this experiment.[23] The difference is about 86 cm^{-1}. Although the experimental result presents a rather large uncertainty ($\pm$480 cm^{-1}), our well depths are deeper compared to the other theoretical ones. We also observe that our calculated dissociation energy agrees well with those obtained by Abe et al.[24] using the CCSD (T) method ($\delta D_e = 2.74\%$) while the relative difference is 6.9% using the CASPT2 method. We also observed that our well depth is slightly lower than that calculated by Aymar et al.[22] however, it is larger than the one obtained by Fuentealba and Reyes. Concerning the vibrational constant, our value is in excellent agreement with Refs. [25] and [26], the remaining difference is very weak, 5.2 cm^{-1}. While there is a somewhat larger difference with the ω_e found by Abe et al.[24] using CCSD (T), it is reduced using CASPT2 (40 cm^{-1}).

The present computed constants R_e, D_e, and ω_e of the $A^1\Sigma^+$, $C^1\Sigma^+$, $D^1\Sigma^+$, and $E^1\Sigma^+$ excited states are close to the ones obtained by Aymar et al.,[22] with the follow relative discrepancies $\delta(R_e) < 0.6\%$, $\delta(D_e) < 0.2\%$, and $\delta(\omega_e) < 0.014\%$. For the $(a-f)^3\Sigma^+$, the comparison with Ref. [22] shows an overall good agreement with differences which do not exceed 150 cm^{-1} for the well depth. Generally, the wells found in Ref. [22] are less deep than those determined here. Furthermore, the deviation found between our equilibrium distances R_e and the ones of Ref. [22] is smaller than 0.4 a.u. We used similar methods than in Ref. [22], therefore, the rather good agreement was expected. However, we have considerably extended the basis set used to allow a much wider exploration, particularly for the high energy states.

Table 2. Spectroscopic constants for $^{1,3}\Sigma^+$, $^{1,3}\Pi$, and $^{1,3}\Delta$ states of the SrH^+ ionic system compared with the available results in the literature.

States	R_e (a.u.)	D_e (cm^{-1})	T_e (cm^{-1})	ω_e (cm^{-1})	$\omega_e\chi_e$ (cm^{-1})	B_e (cm^{-1})	Reference
(a) $^1\Sigma^+$ States							
$X^1\Sigma^+$	3.72	17588	0	1351.2	19.131	4.365	This work
	3.73	18078	–	1429.0	–	–	Aymar et al. [22]
	–	17502±480	–	–	–	–	Dalleska et al. [23]
	3.87	16375	–	1397.3	–	4.072	Abe et al. [24] CASPT2
	3.85	17105	–	1408.8	–	4.094	Abe et al. [24] CCSD(T)
	3.85	15969	–	1346.0	–	–	Fuentealba et al. [25]
	3.93	16088	–	1346.0	–	–	Schilling et al. [26]
$A^1\Sigma^+$	4.64	8843	19845	728.8	5.248	2.806	This work
	4.67	8830	–	712.0	–	–	Aymar et al. [22]
$C^1\Sigma^+$	5.77	6462	29135	419.3	−2.263	1.814	This work
	5.81	6098	–	359.0	–	–	Aymar et al. [22]
$D^1\Sigma^+$	8.29	10064	54497	505.1	4.509	0.879	This work
	8.29	10140	–	510.0	–	–	Aymar et al. [22]
$E^1\Sigma^+$	5.70	6135	58605	551.6	56.095	1.859	This work
	5.72	6229	–	599.0	–	–	Aymar et al. [22]
$F^1\Sigma^+$	4.64	2930	65566	287.9	16.142	2.805	This work
2^{nd}min	13.62	1725					
$G^1\Sigma^+$	5.46	6804	68297	181.4	2.638	2.026	This work
2^{nd}min	15.51	5575					
$H^1\Sigma^+$	5.29	2409	74099	393.6	11.137	2.159	This work
2^{nd}min	8.25	5219					
$I^1\Sigma^+$	5.21	3612	75720	172.3	5.207	2.225	This work
2^{nd}min 3^{rd}min	6.54	4096					
	21.95	2455					
$J^1\Sigma^+$	4.89	2422	77130	312.3	10.675	2.526	This work
2^{nd}min	6.26	4007					
3^{rd}min	11.51	1659					
4^{rd}min	26.32	1071					
$K^1\Sigma^+$	6.00	6284	78272	203.6	6.096	1.678	This work
2^{nd}min	28.62	4338					
$L^1\Sigma^+$	5.84	8307	80627	448.9	14.550	1.771	This work
$M^1\Sigma^+$	5.65	6945	82644	289.4	5.755	1.892	This work
2^{nd}min	32.35	842					
$N^1\Sigma^+$	5.51	5545	84127	321.5	8.543	1.989	This work
2^{nd}min	10.36	3896					
(b) $^3\Sigma^+$ States							
$a^3\Sigma^+$	8.04	155	11493	88.3	13.600	0.934	This work
	8.45	88	–	78.0	–	–	Aymar et al. [22]
$c^3\Sigma^+$	8.91	102	26201	62.4	10.260	0.834	This work
	9.30	44	–	46.0	–	–	Aymar et al. [22]
$d^3\Sigma^+$	11.77	37.97	39630	32.0	12.006	0.436	This work
	12.00	19.00	–	38.0		–	Aymar et al. [22]
$e^3\Sigma^+$	4.63	2849	57656	683.7	31.480	2.818	This work
	4.65	2838	–	876.0		–	Aymar et al. [22]
$f^3\Sigma^+$	4.59	2647	64259	752.0	18.485	2.867	This work
	4.57	2801	–	584.0	–	–	Aymar et al. [22]
$g^3\Sigma^+$	5.41	1855	65693	456.8	−9.335	2.064	This work
$h^3\Sigma^+$	5.15	2994	73720	473.6	16.939	2.277	This work
$i^3\Sigma^+$	4.90	4764	74958	541.7	15.886	2.516	This work
2^dmin	10.45	1211					
$j^3\Sigma^+$	4.78	3296	77781	569.9	43.561	2.644	This work
2^{nd}min	8.91	1866					
3^{rd}min	12.31	348					
$k^3\Sigma^+$	5.11	6432	78821	393.1	12.395	2.313	This work
2^dmin	10.37	4517					
$l^3\Sigma^+$	5.02	6718	82597	195.4	1.377	2.397	This work
2^dmin	8.99	7483					
$m^3\Sigma^+$	5.11	6396	83265	148.9	0.128	2.313	This work
2^dmin	8.07	5819					
3^{rd}min	12.92	4747					
$n^3\Sigma^+$	4.75	3502	85800	268.0	5.434	2.677	This work
2^dmin	7.32	5744					
$o^3\Sigma^+$	5.51	2910	87183	339.2	7.602	1.989	This work
2^dmin	7.02	3884					
$p^3\Sigma^+$	5.31	6575	87487	115.3	0.880	2.142	This work
2^dmin	23.65	3143					

TABLE 2. *Continued*

States	R_e (a.u.)	D_e (cm^{-1})	T_e (cm^{-1})	ω_e (cm^{-1})	$\omega_e\chi_e$ (cm^{-1})	B_e (cm^{-1})	Reference
(c) $^{1,3}\Pi$States							
$B^1\Pi$	5.77	3476	25704	219.9	28.570	1.814	This work
	5.85	3524	–	207.0	–	–	Aymar et al. [22]
$b^3\Pi$	4.52	2182	24163	607.8	43.264	2.957	This work
	4.94	2125		619.0	–	–	Aymar et al. [22]
$1^1\Pi$	5.13	1239	34330	404.8	35.277	2.295	This work
	5.14	1150		410.0	–	–	Aymar et al. [22]
$1^3\Pi$	4.92	2196	33405	552.3	34.543	2.496	This work
	4.95	2095		541.0	–	–	Aymar et al. [22]
$2^1\Pi$	4.95	2383	62289	563.2	32.179	2.465	This work
	4.97	2350		559.0	–	–	Aymar et al. [22]
$2^3\Pi$	5.18	3143	61512	497.5	18.277	2.251	This work
	5.20	3087		495.0	–	–	Aymar et al. [22]
$3^1\Pi$	5.07	2160	65125	484.3	26.910	2.350	This work
$3^3\Pi$	5.00	2218	65074	496.2	29.624	2.416	This work
$4^1\Pi$	4.82	7384	71597	625.6	11.533	2.600	This work
$4^3\Pi$	4.91	9052	69870	599.2	8.347	2.505	This work
$5^1\Pi$	5.00	3588	76513	516.7	29.264	2.416	This work
$5^3\Pi$	5.06	3878	76,215	529.6	26.398	2.359	This work
$6^1\Pi$	5.05	11015	77778	234.1	1.045	2.368	This work
$6^3\Pi$	5.03	11026	77775	207.6	0.454	2.387	This work
$7^1\Pi$	5.06	7946	81562	469.4	6.924	2.359	This work
$7^3\Pi$	5.10	8461	80807	480.9	8.003	2.322	This work
$8^1\Pi$	5.00	7176	86484	229.7	4.367	2.600	This work
$8^3\Pi$	5.09	3424	86082	270.8	3.129	2.331	This work
	7.43	4499					
$9^3\Pi$	5.09	6247	87405	162.3	2.620	2.332	This work
	6.31	6345					
	13.08	4249					
(d) $^{1,3}\Delta$States							
$1^1\Delta$	5.32	856	25193	335.8	35.990	2.134	This work
	5.33	761		336.0	–	–	Aymar et al. [22]
$1^3\Delta$	5.29	885	25157	594.6	−203.474	2.158	This work
	5.30	794		345.0	–		Aymar et al. [22]
$2^1\Delta$	5.05	1973	62678	508.7	34.395	2.368	This work
	5.07	1902		487.0	–	–	Aymar et al. [22]
$2^3\Delta$	5.05	1978	62672	487.8	30.623	2.368	This work
	5.06	1908		486.0	–	–	Aymar et al. [22]
$3^1\Delta$	5.04	2235	76635	497.2	28.279	2.378	This work
$3^3\Delta$	5.04	2238	76635	552.2	37.536	2.378	This work
$4^1\Delta$	4.61	4137	85858	1054.0	78.211	2.842	This work
$4^3\Delta$	4.39	4168	85980	996.6	68.631	3.134	This work
$5^3\Delta$	5.05	7350	86635	991.9	16.730	2.041	This work
2^dmin	8.57	2869					

The data reported in Table 2 (a, b) correspond to the first theoretical determination for the (F-N)$^1\Sigma^+$ and (g-p)$^3\Sigma^+$ excited states. The $H^1\Sigma^+$ and $g^3\Sigma^+$ states have a weak first well depth. The $I^1\Sigma^+$ adiabatic state has a triple minima potential shape, with a well at wide internuclear distances (21.95 a.u.) and two other wells at short distances (5.21 and 6.54 a.u.). As previously discussed, the unusual shape of this state is the result of three avoided crossing in its potential curve as shown in Supporting Information, Table S1.

For Π symmetry, the molecular spectroscopic parameters are listed in Table 2 (c). We observe again a good agreement with those computed by the *ab initio* calculations of Aymar et al.[22] However, we found slightly greater equilibrium distances. For the equilibrium distance of (1 and 2) $^{1,3}\Pi$ states, the difference is less than 0.03 a.u., whereas for the well depth and vibrational constant, the difference does not exceed 100 and 10 cm^{-1}, respectively. The same analysis is valid for both $B^1\Pi$ and $b^3\Pi$ states. This was expected since we used similar methods. Concerning the highest states (3–9)$^{1,3}\Pi$, this work is the first study, to our knowledge.

Table 2 (d) shows the spectroscopic constants related to Δ symmetry. Obviously, the data reported by Aymar et al. agrees well with our results. All spectroscopic parameters for triplet and singlet Δ dissociating toward the same dissociation limits are almost equal, specially for (1, 2, and 3) $^{1,3}\Delta$, and numerically confirms the quasi degeneracy shown in the corresponding PECs (seen in Fig. 4).

Globally, our PECs have a shape similar to those obtained by Aymar et al. The differences are mainly in details of the spectroscopic constants listed in Table 2 (a–d). This is not surprising since we used the same procedures (ECP and CPP). However, in addition to the much larger basis set used here,

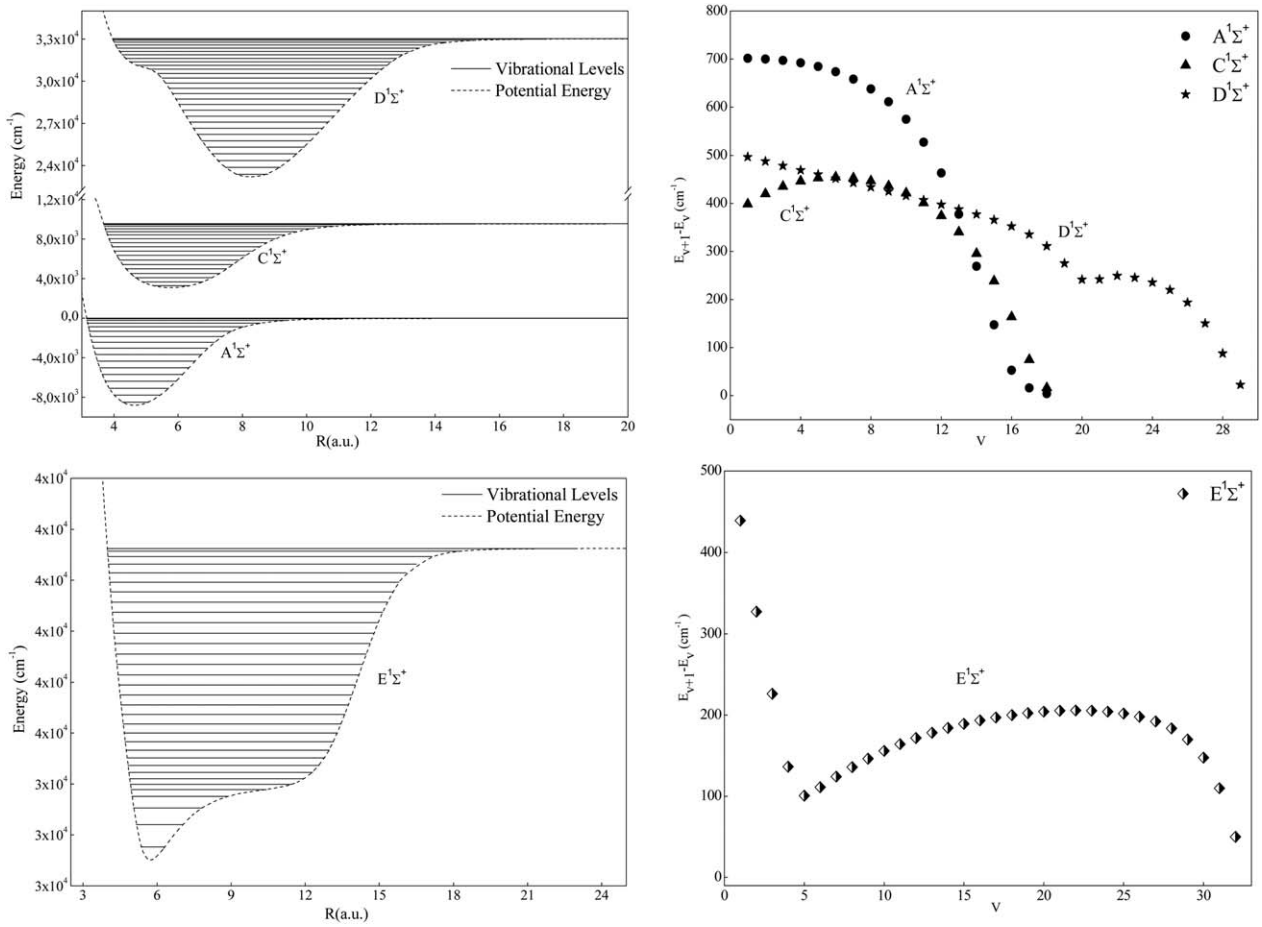

Figure 5. Potential energy curves with their vibrational levels (left) and vibrational levels spacing (right) for $A^1\Sigma^+$, $C^1\Sigma^+$, $D^1\Sigma^+$, and $E^1\Sigma^+$ states.

Aymar et al. used the CPP in the *l*-dependent version (ρ_s= 2.134, ρ_p= 2.183, and ρ_d= 1.704 a.u.) while we used a single cutoff radius (ρ= 2.3995 a.u.).

Vibrational levels

To motivate further experimental or theoretical spectroscopic studies and to get insight for the properties of the SrH^+ ion, we have computed in the adiabatic representation the vibrational levels for numerous states of symmetries Σ^+, Π and Δ. The resolution of the radial Schrödinger equation was done using a Numerov algorithm with the trial energies supplied by a pseudospectral approach.

Figure 5 illustrates the PECs for the $A^1\Sigma^+$, $C^1\Sigma^+$, $D^1\Sigma^+$, and $E^1\Sigma^+$ with its vibrational levels as well their spacing ($E_{v+1} - E_v$) as a function of the vibrational quantum number. For the $A^1\Sigma^+$ state, the spacing of the low vibrational levels presents a linear behavior, which is assigned to a Morse like anharmonic form in the PEC. After a progressive diminution, the spacing vanishes at the dissociation limit Sr^+ (4d) + H (1s). The same interpretations are also valid for all states which have a single well depth such as the $C^1\Sigma^+$. While for $E^1\Sigma^+$, the spacing presents a linear behavior up to $v = 5$ related to an anharmonic potential in the vicinity of the equilibrium distance. Then, an abrupt behavior is observed. It reflects a widening in the well and the levels become denser above $v = 5$. We can see the same behavior in the $D^1\Sigma^+$ state with an abrupt variation around $v = 20$. For the $E^1\Sigma^+$ and $C^1\Sigma^+$ states, we observe a prominent motif with a set of vibrational spacings that are gradually increasing across a broad range of *v*. This is a very unusual behavior related to quite unusual shapes for these potentials imprinted by various avoided crossing.

In Supporting Information, Table S2, we give the vibrational level spacing ($E_{v+1} - E_v$) for the other excited states of symmetry $^1\Sigma^+$. Almost all states present strong anharmonic effects. Moreover, a roughly linear decreasing behavior is observed at the beginning, followed by a sharper decrease. Then, when reaching the dissociation limit, the vibrational spacing presents a regular variation, as usual for ionic systems dominated by asymptotic behaviors in C_4/R^4.

As depicted in Figure 6a, the spacing of the highest states with several wells may present abrupt variations because the anharmonic progression in each well may even produce quasi-degeneracies. We obtained 96 and 65 vibrational levels for the (K and L) $^1\Sigma^+$ states, respectively, and fewer vibrational levels for the other states as shown in Supporting Information, Table S3. The $H^1\Sigma^+$ state present an interesting behavior [Table 2 (a)]: we note a smooth anharmonic shape below $v = 13$, then

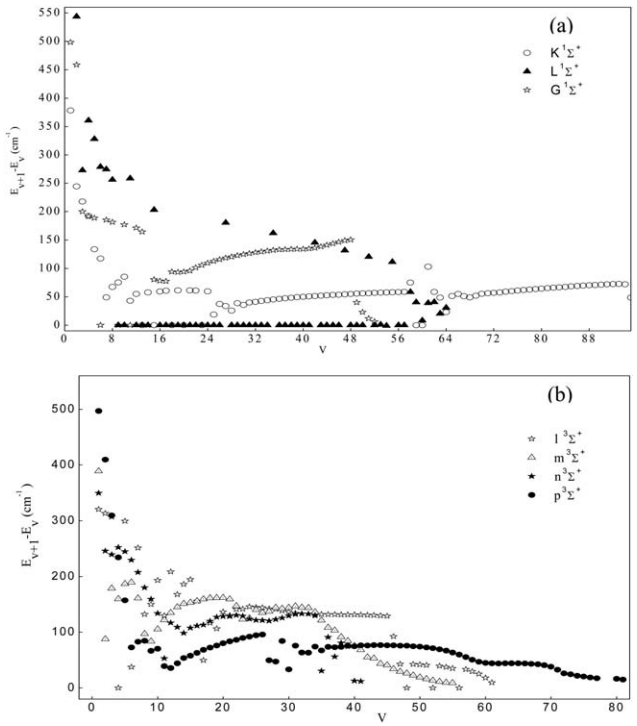

Figure 6. Vibrational level spacings: (a) for (K, L, G)$^1\Sigma^+$ states and (b) for (I, m, n, p)$^3\Sigma^+$ states.

a sudden change reflecting an enlargement in the well where the vibrational levels are numerous and tightened. A very unusual behavior can also be seen for the $J^1\Sigma^+$ state. For this state, there are clearly three progressions, one for the five lower vibrational levels, the second between $v = 6$ and $v = 16$ and the third one for the higher levels with an accidental quasidegeneracy clearly seen in the vibrational spacing progression here ($v = 14$, 16). For $G^1\Sigma^+$, we also observe unusual behaviors which can be related to the two separate wells in their electronic potential. The inner well is narrower and leads to a wider spacing while the outer well is wider and leads to much lower vibrational spacings. A similar behavior can be observed also for the $I^1\Sigma^+$, $M^1\Sigma^+$, and $J^1\Sigma^+$ states, however, to a lower extent because the inner well is not as deep as that in the $G^1\Sigma^+$ state case and, therefore, the related progression only extends to a few vibrational levels and tunneling through the barrier helps merging the two progressions.

Supporting Information, Table S4 summarizes the ($E_{v+1} - E_v$) vibrational spacing of the $X^1\Sigma^+$ and the (a−o)$^3\Sigma^+$ states. The ground state contains 22 vibrational levels while Abe et al.[24] found 18 vibrational levels in their potential well with a CASPT2 method. We note the presence of very repulsive states as $a^3\Sigma^+$, $c^3\Sigma^+$, $d^3\Sigma^+$, $e^3\Sigma^+$, $f^3\Sigma^+$, and $g^3\Sigma^+$ which possess only a few levels, whereas $h^3\Sigma^+$, $i^3\Sigma^+$, and $j^3\Sigma^+$ trap numerous vibrational levels as they have deeper potential wells as indicated in Supporting Information, Table S3. The potential wells of the $d^3\Sigma^+$ state are wide but not deep ($D_e = 37.97$ cm^{-1}). That is why it contains only two vibrational levels (as can be seen in Supporting Information, Table S3). For the majority of $^3\Sigma^+$ states, we observe in Figure 6b that the vibrational level spacings are not regular due to the avoided crossing seen previously in their PECs (Figs. 2a and 2b). Interestingly, the spacing between the vibrational levels of the $p^3\Sigma^+$ state, which has 82 levels, show a sudden change explained by the emergence of a second well. The latter is wider as it presents a slow variation for the first vibrational levels and it leads to much lower vibrational spacing. For all other states with a double well, we notice similar observations, in particular for $n^3\Sigma^+$.

We have reported in Supporting Information, Table S5, the spacing of the higher excited states of $^{1,3}\Pi$ symmetry. The data reported in Supporting Information, Table S6 corresponds to the spacing of vibrational levels for symmetries Δ. We note that the singlet and triplet Delta states dissociating to the identical limit have almost the same number of vibrational levels and almost the same spacing. The $5^3\Delta$ has a deep potential well that contains 25 levels, while both $1^1\Delta$ and $1^3\Delta$ states contain only seven vibrational levels.

Properties of electric dipole moment

The transition rates calculations between vibrational levels for the alkaline earth hydride ions, as needed for measuring of the proton-to-electron mass ratio requires a good knowledge of the electric dipoles properties.[71,72] The computed PDM value of the ground state for these cations provides estimation for the associated Stark shifts.[24] In addition the good quality calculations of electric dipole properties (PDM) on molecules such as CaH^+, BaH^+, and MgH^+ are very interesting and constitute the first step to illustrate the repartition of charges in the adiabatic states.[14,16,55,73] Consequently, we have investigated the PDM and TDM functions of SrH^+ for all states bellow the ionic limit mainly to better know the ionic character of the $^1\Sigma^+$ states at the vicinity of the avoided crossing and in the other symmetries also. The computation of this quantity depends on the choice of the origin for the calculation. Here, the center of the strontium atom is chosen as origin and H moves along the positive side of the R axis. Therefore, at large R, only the charge on H matters, the states corresponding to (Sr^*+H^+) tend toward the ($+R$) line, the ones related to ($Sr^{*+}+H$) tend toward the R axis and those corresponding to the double charge transfer ionic state ($Sr^{2+} + H^-$) tend toward the ($-R$) line.

Figure 7 illustrates the PDM of the $^1\Sigma^+$ states (the PDM values given in Supporting Information, Table S7). The PDM of $^1\Sigma^+$ states vary quite much. For short distances, they present large variations but small amplitudes, whereas more abrupt variations can be seen at large distances with large amplitudes. Noteworthy, one after the other, almost each adiabatic state possesses its dipole moment that reaches the curve ($-R$) and then falls to zero when the next state's curve increases to recover the next piece of the ($-R$) curve, and crossings now evidently appear. When combined, these pieces give a good account of ($-R$) function that characterizes the double charge transfer ionic state ($Sr^{2+} + H^-$). The G state which dissociates to Sr ($5s^2$) + H^+ clearly behaves at large distance in $+R$, as expected. Actually this behavior is reached after the weakly

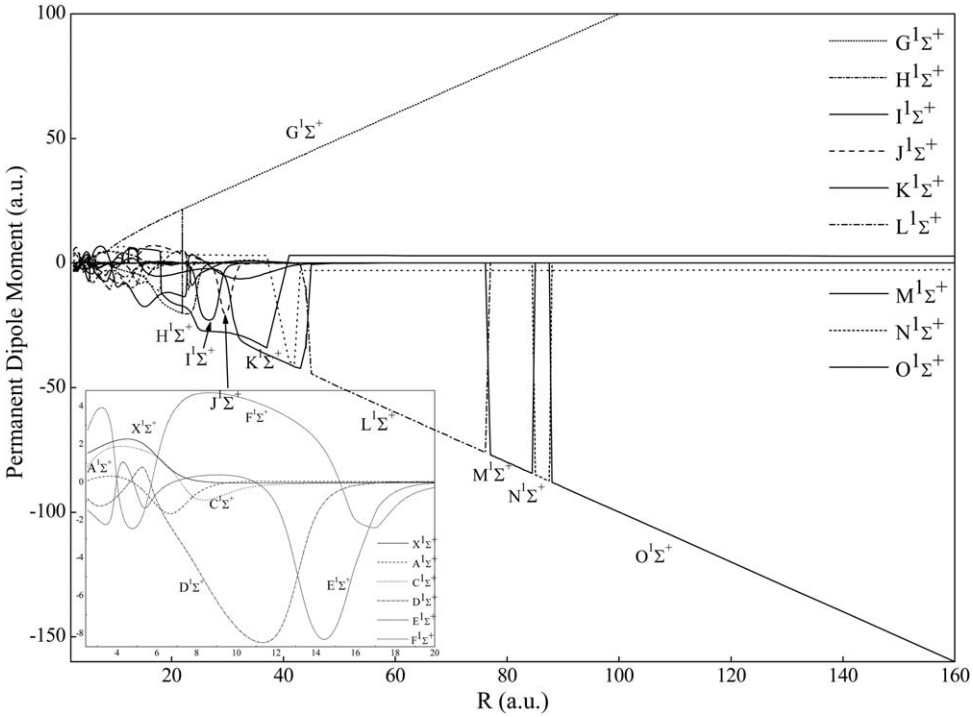

Figure 7. Global picture of the permanent dipole moment of the $^1\Sigma^+$ states.

avoided crossing around 22 a.u. It is clear that these variations of the PDM are induced by the changes in the electronic wave function. They can be very sharp, especially at large distances when related to weakly avoided crossing in the potentials. We note also that the crossings seen in the dipole moment curves coincide with the crossings positions previously seen in the PECs. The PDM can, thus, give interesting information about the physical nature of the states as for the molecules CaH^+, BaH^+, and MgH^+.[14,16,55,59] Let us recall that the avoided crossing may have significant role for the excitation or charge transfer efficiency. Therefore, these data could be useful in the modeling of collisions between laser-cooled and trapped calcium, magnesium, strontium, and barium cations and H_2 systems.[43]

The PDM curves for $^3\Sigma^+$ are drawn in Figures 8a and 8b. They are far from constant and present interesting behaviors. Figure 8a shows the important variations at short distances below 15 a.u. In this region, the dipole moments are not negligible at all, and become particularly important for the highly excited states. When R is larger, the dipole moment curves vanish and asymptotically reach zero, as expected for the $Sr^{*+} + H$ states. For example, the $c^3\Sigma^+$ state presents a maximum $\mu_{max} = 1.72$ a.u. at the distance $R = 3.67$ a.u., then it slowly decreases. For the $g^3\Sigma^+$ state, it increases at shorter distances from $\mu_{max1} = -2.98$ a.u. to $\mu_{max2} = +5.62$ a.u. then it decreases until an extrema of $\mu_{max3} = -2.97$ a.u. before progressively tending toward zero. We see clearly in Figure 8b, two asymptotic behaviors in the PDM curves: $(+R)$ for the electronic states dissociating to $Sr + H^+$ and zero for the $Sr^{*+} + H$ states ones. The PDM curves vary abruptly at large internuclear distances, however, more softly at short distances.

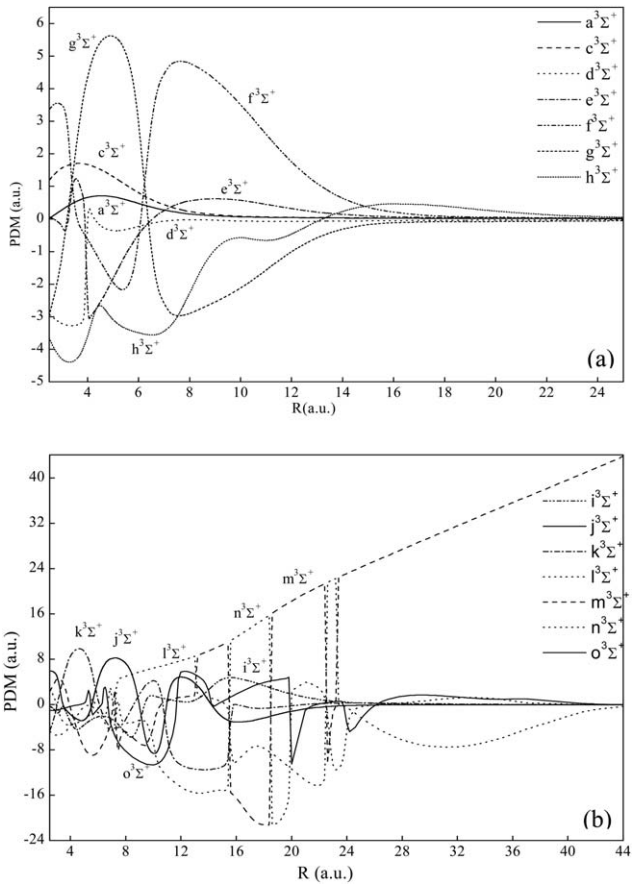

Figure 8. Permanent dipole moment: (a) for (a–h)$^3\Sigma^+$ states at short distances before 15 a.u. and (b) for the highest excited state of $^3\Sigma^+$ states.

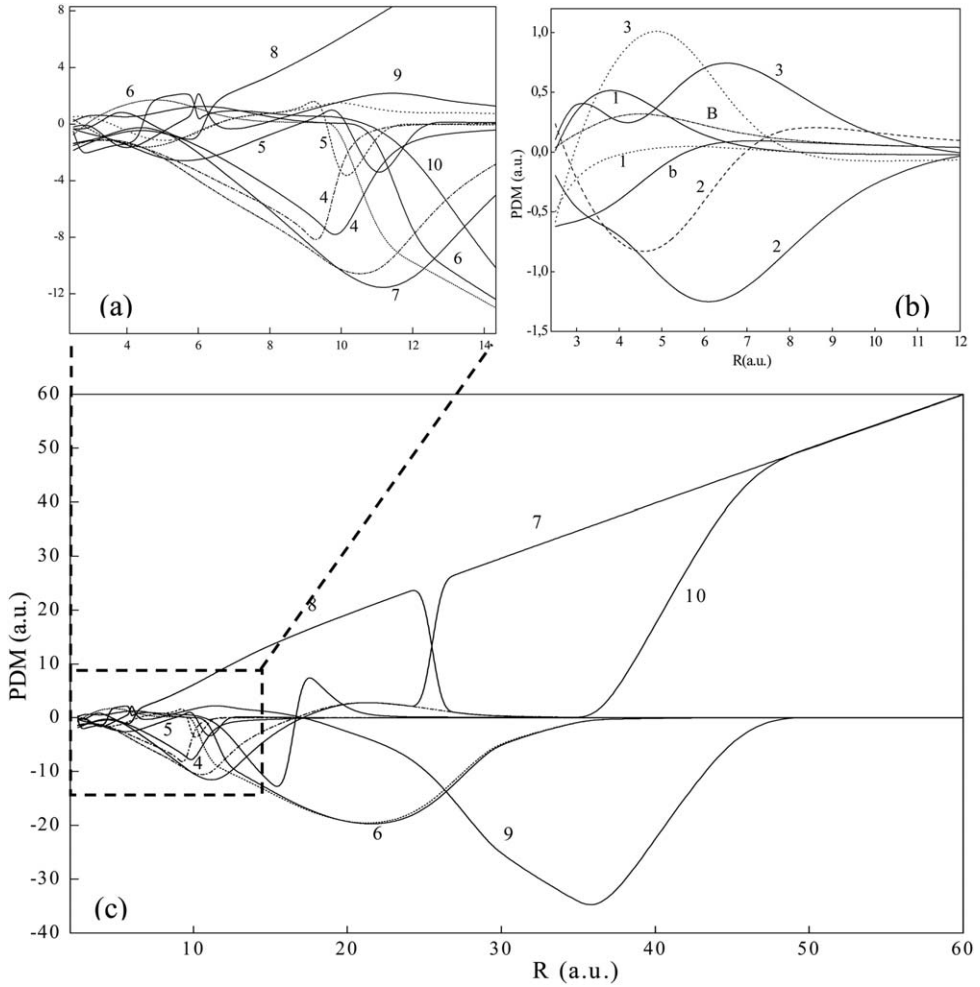

Figure 9. Permanent dipole moment of the $^1\Pi$ (. . .) and $^3\Pi$ (—) states. (a) Zoom picture for the PDM function at short distances. (b) PDM function for (1, b, 2, 3) $^{1,3}\Pi$ at short distances before 12 a.u. (c) Global picture for the PDM function of $^{1,3}\Pi$.

Conversely, we can say that these figures clearly illustrate a behavior similar to the one of the $^1\Sigma^+$ states. However, the situation is more complex, the PDM functions are much weaker than for the $^1\Sigma^+$ and no ionic states with H^- were expected here. Surprisingly, we also see for *R* between 10 and 20 a.u. some states with large and negative PDM, compatible with a $Sr^{2+} + H^-$ imprint. Moreover, these states are the ones behaving like an ionic state in the potential curves. Therefore, potentials and PDM seem to corroborate the existence of $Sr^{2+}+H^-$ states in $^3\Sigma^+$ symmetry, at intermediate distances, in the higher energy part.

The PDM curves for the states belonging to $^{1,3}\Pi$ symmetry are mentioned in Figures 9a–9c. As indicated in these figures, the PDM for the Π symmetry are also rather considerable and

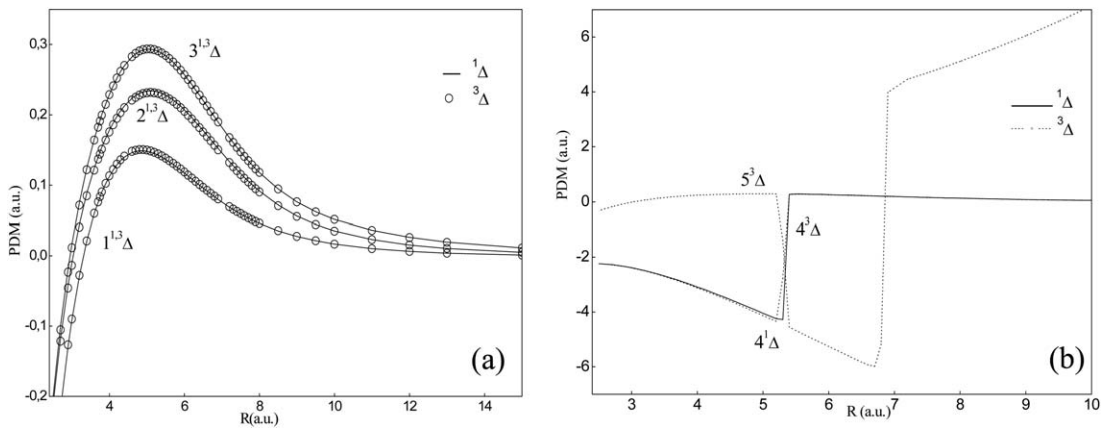

Figure 10. Permanent dipole moment of the $^{1,3}\Delta$ states.

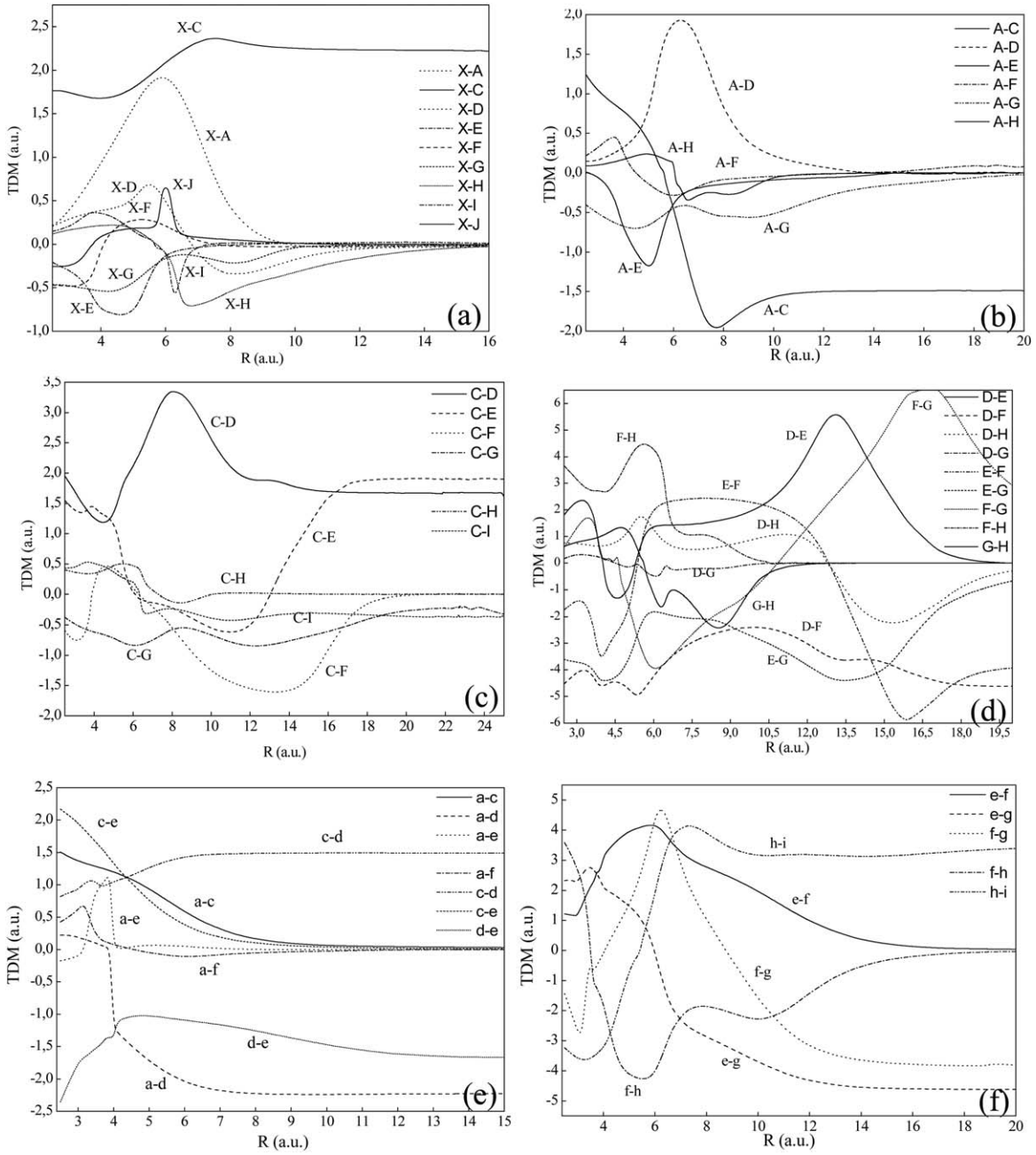

Figure 11. Transition dipole moment for selected excited states with symmetry $^{1,3}\Sigma^+$.

become especially significant for high states. When R is larger, the electric dipole moment for $(1–4)^{1,3}\Pi$ asymptotically reaches zero for $Sr^{*+}+H$ sates, or to $+R$ for the $Sr^* + H^+$ ones. Again, while for the excited states the variation of PDM is softer at short distances, it is brutal at larger ones. We also see some imprint of $Sr^{2+} + H^-$ states between 10 and 40 a.u.

Turning now to $^{1,3}\Delta$ symmetries (Figs. 10a and 10b), the maxima of PDM functions are situated in the range of interatomic distances $4 \leq R \leq 7$ a.u. and the PDM of the triplet and singlet states have almost the same shape, at least for (1–3) $^{1,3}\Delta$. At larger distances, they vanish, as expected. Interestingly, it can be observed that the adiabatic dipole moments of the $4^3\Delta$ and $5^3\Delta$ states present abrupt variations at $R = 5.3$ a.u. related to a weakly avoided crossing between their PECs (Fig. 4). Again, some imprint of $Sr^{2+} + H^-$ can be seen for the 4 and 5 high excited states. It is worth mentioning that the highest state present an abrupt change at $R = 5.32$ a.u. and switches from an H^- to an H^+ character as clearly indicated by its PDM, which switches from a large negative value to a large positive one.

In addition, we have determined the TDM functions of SrH^+ for several states below the ionic limit. Figures 11a–11d, illustrates the TDM from $X^1\Sigma^+$ to the ninth excited states $(A-G)^1\Sigma^+$ as well as between some other excited states of $^1\Sigma^+$ symmetry. A meaningful variation has been noted from these functions as it may be linked to the huge number of avoided crossing found in the potentials. In particular, the positions of the extrema of the TDM curves can be assigned to the avoided crossing positions. As an illustration, the transition

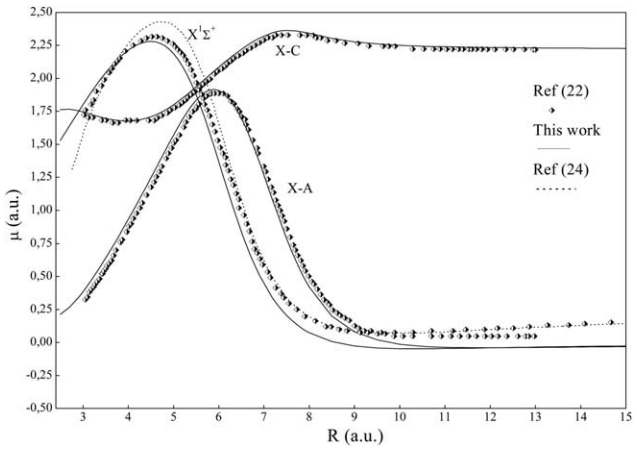

Figure 12. TDM and PDM curves compared to those obtained by Aymar et al. [22] and Abe et al. [24].

$(F–G)^1\Sigma^+$ falls from 1.64 to −3.96 a.u. in the interval of interatomic distance $R = [3.47, 6]$, then it raises to a maximum of +6.52 a.u. reached at $R = 16.52$ a.u. (Fig. 11d). This behavior can be understood when correlated to the presence of a three avoided crossing between these two states. A similar behavior is observed for the $(D–E)^1\Sigma^+$ transition. We note that several transitions did not decline to zero at larger internuclear distance but asymptotically reached the corresponding allowed atomic transition, for instance the transition among $(C–D)^1\Sigma^+$, $(X–C)^1\Sigma^+$, and $(A–C)\ ^1\Sigma^+$. For the triplet sigma state, the TDM curves are depicted in Figures 11e and 11f. The most important transition is between the $(f–g)^3\Sigma^+$. The $(e–f)\ ^3\Sigma^+$ transition is also rather strong and has a maximum of 4.2 a.u. at $R = 5.9$ a.u.

In Figure 12, our results for the PDM of the ground state and the TDM curves for the $(X–A^1\Sigma^+, X–C^1\Sigma^+)$ transitions are compared to those calculated in Refs. [22] and [24]. As to $X^1\Sigma^+$, we observe that the three plotted curves present quite alike behaviors. Our maximum of PDM is between the maximum obtained by Abe and by Aymar, with differences about 0.3 a.u. The behavior is slightly different at large distances, probably due to the different choice of the origin. Concerning the TDM results, the maximum of $(X–A)^1\Sigma^+$ transition obtained by Ref. [22] is of 0.04 a.u. longer than our maximum, but the curves are very similar both for $(X–A)\ ^1\Sigma^+$ and $(X–C)\ ^1\Sigma^+$ TDM.

Conclusion

In this work, we have carried out a quantum *ab initio* calculation to describe the electronic structure of the ionic molecule SrH^+, in the adiabatic representation, for all electronic states below $(Sr^{2+} + H^-)$. The *ab initio* approach is based on nonempirical relativistic pseudopotential for the strontium core, complemented by operatorial core valence correlation estimation with parameterized CPP and FCI methods. Extended GTO basis sets have been optimized for both atoms (Sr and H) to reproduce the experimental energy spectra for 20 atomic levels with a good accuracy.

The PECs and their corresponding spectroscopic parameters were evaluated for almost all the 34 $^{1,3}\Sigma^+$, 20 $^{1,3}\Pi$, and 9 $^{1,3}\Delta$ states. A good agreement has been obtained with the available spectroscopic constants theoretically studies [22–26] confirming the validity of our approach and making reliable the large amount of new results.

Interestingly, the $^1\Sigma^+$ states present an important series of avoided crossing. Their highly potential energy is strongly imprinted by the ionic state $Sr^{2+}\ H^-$ like for BaH^+, CaH^+ and MgH^+ systems.[14,15,59] The multiplicity of crossings leads to unusual potential shapes with various wells which may trap vibrational levels in various R ranges. Interesting effects can be expected for the charge or excitation transfers efficiency at the crossings which could be of great interest in various astrophysical conditions.

In addition, the dipole moments for all the states were also considered. Through an analysis of electric dipole moment, the avoided crossing positions indicated in the potentials can be fixed. At the vicinity of these positions, the behaviors of TDM between two adjacent states present considerable change. The ionic character for various adiabatic states is well shown by the behavior of the PDM and PEC, which piecewise reproduces the expected $(-R)$ curve for the PDM and the $(-2/R)$ curve for the PECs.

We have found quite unusual forms of the potentials with multiple wells for various states, and even accidental degeneracy in their vibrational progression and we have seen strong anharmonic effects. For the quantum dynamics of reactions like $[(X^+)^* + H_2 \rightarrow XH^+ + H]$ (with X = Be, Mg, Ca, Sr, Ba), our results may be considered as a necessary step toward the modeling of these reactive collisions between trapped cold alkaline earth (Mg^+, Ba^+, Sr^+,...) cations and H_2 molecules, as in the reaction $[(Mg^+)^* + H_2 \rightarrow MgH^+ + H]$ [43]. Surprisingly, $Sr^{2+} + H^-$ states have also been found in unexpected symmetries: $^3\Sigma^+$, $^{1,3}\Pi$ and $^{1,3}\Delta$ in the high energy potential curves and corroborated by large and negative PDM. Such states will probably autoionize at larger interatomic distances and could be stabilized by the proximity of the double positive charge on Sr. Similar states were also found for the MgH^+ molecular ion.[59]

Noteworthy, inspection of the highly PECs shows that it seems possible to neutralize H^+ or even to produce H^- in single collisions with strontium. This process could be of critical significance in specific astrophysical conditions.

Beyond their intrinsic interests, we hope that the present results will motivate and help future experimental or theoretical investigations in spectroscopy or collision fields.

Keywords: Adiabatic potential energy · vibrational levels · spectroscopic proprieties · electric dipole moment

How to cite this article: H. Habli, L. Mejrissi, N. Issaoui, S. J. Yaghmour, B. Oujia, F. X. Gadéa. *Int. J. Quantum Chem.* **2014**, DOI: 10.1002/qua.24813

Additional Supporting Information may be found in the online version of this article.

[1] E. GharibNezhad, A. Shayesteh, P. F. Bernath, *Mon. Not. R. Astron. Soc.* **2013**, *432*, 2043.
[2] M. Mostafanejad, A. Shayesteh, *Chem. Phys. Lett.* **2012**, *551*, 13.

[3] R. Celiberto, K. L. Baluja, R. K. Janev, *Plasma Sources Sci. Technol.* **2013**, *22*, 015008.
[4] P.J. Bruna, F. Grein, *Phys. Chem. Chem. Phys.* **2003**, *5*, 3140.
[5] T. C. Steimle, C. Jinhai, *G. Jamie. J. Chem. Phys.* **2004**, *121*, 829.
[6] D. Ben Abdallah, F. Najar, N. Jaidane, Z. Ben Lakhdar, N. Feautrier, A. Spielfiedel, F. Lique, *Chem. Phys. Lett.* **2009**, *473*, 39.
[7] A. Shayesteh, R.D.E. Henderson, R.J. Le Roy, P.F. Bernath, *J. Phys. Chem. A* **2007**, *111*, 12495.
[8] A. Shayesteh, K.A. Walker, I. Gordon, D.R.T. Appadoo, P.F. Bernath, *J. Mol. Struct.* **2004**, *695–696*, 23.
[9] A. Boutalib, J. P. Daudey, M. El Mouhtadi, *Chem. Phys.* **1992**, *167*, 111.
[10] F. B. C. Machado, F. R. Ornellas, *J. Chem. Phys.* **1991**, *94*, 7237.
[11] L. F. Errea, B. Herrero, L. Mendez, I. Rabadan, P. Sanchez, *J. Phys. B: At. Mol. Opt. Phys.* **1994**, *27*, L753.
[12] M. Abe, Y. Moriwaki, M. Hada, M. Kajita, *Chem. Phys. Lett.* **2012**, *521*, 31.
[13] A. K. Belyaev, P. S. Barklem, A. Spielfiedel, M. Guitou, N. Feautrier, D. S. Rodionov, D.V. Vlasov, *Phys. Rev. A.* **2012**, *85*, 032704.
[14] L. Mejrissi, H. Habli, H. Ghalla, B. Oujia, F.X. Gadéa, *J. Phys. Chem. A.* **2013**, *117*, 5503.
[15] H. Habli, H. Ghalla, B. Oujia, F. X. Gadéa, *Eur. Phys. J. D.* **2011**, *64*, 5.
[16] H. Habli, R. Dardouri, B. Oujia, F. X. Gadéa, *J. Phys. Chem. A.* **2011**, *115*, 14045.
[17] G. Ohanessian, M. J. Brusich, W. A. Goddard, III, *J. Am.Chem. Soc.* **1990**, *112*, 7179.
[18] P. Fuentealba, O. Reyes, H. Stoll, H. Preuss, *J. Chem. Phys.* **1987**, *87*, 5338.
[19] A.R. Allouche, F. Spiegelmann, M. Aubert-Frécon, *Chem. Phys. Lett.* **1993**, *204*, 343.
[20] K. Chakrabarti, J. Tennyson, *Eur. Phys. J. D.* **2012**, *66*:31, 2.
[21] R. Celiberto, R.K. Janev, D. Reiter, *Plasma Phys. Controlled Fusion* **2012**, *54*, 035012.
[22] M. Aymar, O. Dulieu, *J. Phys. B: At., Mol. Opt. Phys.* **2012**, *45*, 215103.
[23] N. F. Dalleska, K. C. Crellin, P. B. Armentrout, *J. Phys. Chem.* **1993**, *97*, 3123.
[24] M. Abe, M. Kajita, M. Hada, Y. Moriwaki, *J. Phys. B: At. Mol. Opt. Phys.* **2010**, *43*, 245102.
[25] P. Fuentealba, O. Reyes, *Mol. Phys.* **1987**, *62*, 1291.
[26] J. B. Schilling, W. A. Goddard, III, J. L. Beauchamp, *J. Am. Chem. Soc.* **1987**, *109*, 5565.
[27] A. J. Sadlej, M. Urban, *THEOCHEM* **1991**, *234*, 147.
[28] T. P. Snow, In *Interstellar Molecules, Proceeding of the IAU Symposium*; B. H. Andrew, Ed.; Reidel: Dordrecht, The Netherlands, **1992**; p. 247.
[29] L. E. Snyder, In Astrochemistry of Cosmic Phenomena, Proceedings of the IAU Symposium; P. D. Singh, Ed.; Kluwer Academic: Dordrecht, The Netherlands, **1992**; p. 427.
[30] C. Arpigny, F. Dossin, J. Manfroid, P. Magain, A. C. Danks, D. L. Lambert, C. Sterken, *Messenger* **1986**, *45*, 8.
[31] P. Sotirovski, *Astron. Astrophys. Suppl.* **1972**, *6*, 85.
[32] L. Wallace, K. Hinkle, G. Li, P. Bernath, *Astrophys. J. Lett.* **1999**, *524*, 454.
[33] J. D. Kirkpatrick, *Annu. Rev. Astron. Astrophys.* **2005**, *43*, 195.
[34] P.L. Gay, D.L. Lambert, *Astrophys. J. Lett.* **2000**, *533*, 260.
[35] H. R. Johnson, A. J. Sauval, *Astron. Astrophys. Suppl. Ser.* **1982**, *49*, 77.
[36] V. L. Ol'shevskii, N. G. Shchukina, I. E. Vasil'eva, *Sol. Phys.* **2008**, *24*, 198.
[37] L. Mashonkina, G. Zhao, T. Gehren, W. Aoki, M. Bergemann, K. Noguchi, J. R. Shi, M. Takada-Hidai, H. W. Zhang, *Astro. Astrophys.* **2008**, *478*, 529.
[38] L. Mashonkina, T. Gehren, I. Bikmaev, *Astro. Astrophys.* **1999**, *343*, 519.
[39] L.I. Antipova, A.A. Boyarchuk, Yu.V. Pakhomov, V.E. Panchuk, *Astron. Rep.* **2004**, *48*, 597.
[40] P. S. Barklem, A. K. Belyaev, A. Spielfiedel, M. Guitou, *N. Feautrier. Astro. Astrophys.* **2012**, *541*, A80.
[41] P. S. Barklem, P. J. O'Mara, *Mon. Not. R. Astron. Soc.* **1998**, *300*, 863.
[42] P.S. Barklem, B.J. O'Mara, *Mon. Not. R. Astron. Soc.* **2000**, *311*, 535.
[43] K. Mølhave, M. Drewsen, *Phys. Rev. A: At. Mol. Opt. Phys.* **2000**, *62*, 1.
[44] P. F. Staanum, K. Højbjerre, R. Wester, M. Drewsen, *Phys. Rev. Lett.* **2008**, *100*, 243003.
[45] A. Bertelsen, I. S. Vogelius, S. Jorgensen, R. Kosloff, M. Drewsen, *Eur. Phys. J. D.* **2004**, *31*, 403.
[46] S. Jørgensen, M. Drewsen, R. Kosloff, *J. Chem. Phys.* **2005**, *123*, 094302.
[47] Ph. Durand, J. C. Barthelat, *Theor. Chem. Acta.* **1975**, *38*, 283.
[48] Ph. Durand, J.C. Barthelat, *Chem. Phys. Lett.* **1974**, *27*, 191.
[49] K. Abdesslem, L. Mejrissi, N. Issaoui, B. Oujia, F.X. Gadéa, *J. Phys. Chem. A.* **2013**, *117*, 8925.
[50] A. Boutalib, F. X. Gadéa, *J. Chem. Phys.* **1992**, *97*, 1144.
[51] F. X. Gadéa, M. Pelissier, *J. Chem. Phys.***1990**, *93*, 545.
[52] M. Groβ, F. Spiegelmann, *Eur. Phys. J. D.* **1998**, *4*, 219.
[53] R. Poteau, F. Spiegelmann, *J. Mol. Spectrosc.* **1995**, *171*, 299.
[54] W. Gaied, H. Habli, B. Oujia, F. X. Gadea, *Eur. Phys. J. D.* **2011**, *62*, 371.
[55] M. Aymar, R. Guéout, M. Sahlaoui, O. Dulieu, *J. Phys. B: At. Mol. Opt. Phys.* **2009**, *42*, 154025.
[56] M. Aymar, R. Guéout, O. Dulieu, *J. Chem. Phys.* **2011**, *135*, 064305.
[57] N. Khelifi, W. Zrafi, B. Oujia, F.X. Gadea, *Phys. Rev. A. At. Mol. Opt. Phys.* **2002**, *65*, 425131.
[58] W. Zrafi, B. Oujia, F. X. Gadea, *J. Phys. B: At. Mol. Opt. Phys.* **2006**, *39*, 3815.
[59] N. Khemiri, R. Dardouri, B. Oujia, F. X. Gadéa, *J. Phys. Chem. A.* **2013**, *117*, 8915.
[60] W. Müller, J. Flesh, W. Meyer, *J. Chem. Phys.* **1984**, *80*, 3297.
[61] H. Coker. *J. Phys. Chem.* **1976**, *80*, 2078.
[62] M. Foucrault, Ph. Millie, J. P. Daudey, *J. Chem. Phys.* **1992**, *96*, 1257.
[63] P. Duplaa, F. Spiegelmann, *J. Chem. Phys.* **1996**, *105*, 1492.
[64] Yu. Ralchenko, A. Kramida, *Reader J and NIST ASD Team 2011 NIST Atomic Spectra Database* (version 4.1). Available at: http://physics.nist.gov/asd/.
[65] C. Pekeris, *Phys. Rev.* **1962**, *126*, 1470.
[66] H. Croft, A. S. Dickinson, F. X. Gadea, *J. Phys. B.* **1999**, *32*, 81.
[67] A. S. Dickinson, R. Poteau, F. X. Gadea, *J. Phys. B.* **1999**, *32*, 5451.
[68] A. K. Belyaev, P. S. Barklem, A. S. Dickinson, F. X. Gadea, *Phys. Rev. A.* **2010**, *81*, 032706.
[69] P. S. Barklem, A. K. Belyaev, A. S. Dickinson, F. X. Gadea, *Astron. Astrophys.* **2010**, *519*, A20.
[70] E. A. Hylleraas, *Astrophys. Norvegica.* **1964**, *9*, 345.
[71] M. Kajita, Y. Moriwaki, *J. Phys. B: At. Mol. Opt. Phys.* **2009**, *42*, 154022.
[72] M. Kajita, M. Abe, M. Hada, Y. Moriwaki, *J. Phys. B: At., Mol. Opt. Phys.* **2011**, *44*, 025402.
[73] H. Berriche, F. X. Gadea, *Chem. Phys. Lett.* **1995**, *247*, 85.

Received: 22 August 2014
Revised: 30 September 2014
Accepted: 29 October 2014
Published online on Wiley Online Library